



Instrument Science Report WFC3 2008-25

WFC3 TV3 Testing: IR Channel Read Noise

B. Hilbert
4 August 2008

ABSTRACT

Using data taken during WFC3's Thermal Vacuum 3 (TV3) testing campaign, we have characterized the readnoise behavior in the IR Channel, which contained IR-4 (FPA165). The Contract End Item (CEI) Specifications call for a correlated double sampling (CDS) readnoise of 15 e^- , along with an achievable readnoise of 10 e^- from a ramp of 10 non-destructive reads. We observe a CDS readnoise of roughly 20.3 – 21.0 e^- , and an effective readnoise of 8.5 – 17 e^- for 16 non-destructive reads, depending on sample sequence. The IR channel meets the spec for achievable readnoise only when using the MIF sample sequences and a line-fitting data reduction technique.

Introduction

The Wide Field Camera 3 (WFC3) underwent a third round of thermal vacuum testing (TV3) during the spring of 2008. This testing was performed using the flight detector, IR-4 (FPA165) in the IR channel. In this test, we report on the readnoise behavior of the flight detector, based on a series of dark current ramps. We examine both the correlated double sampling (CDS) readnoise, as well as the effective noise in ramps composed of more than 2 readouts of the detector.

Data

The data collected and analyzed for this study were the products of several Science Mission Specification (SMS) scripts. These scripts were designed to collect dark current data for the IR channel. They exercised all of the full-frame and a subset of the subarray

sampling sequences available to WFC3 general observers. Details of the timing pattern associated with each sample sequence are given in Petro, 2006. Regardless of sample sequence, each data file contained a ramp composed of 16 non-destructive reads. Table 1 lists the characteristics of the data used for this readnoise analysis.

SMS	Sample Sequence	Full Ramp Exposure Time (sec)	Subarray Sizes (pixels)	Num. of Ramps MEB1/MEB2
IR01S03	RAPID	44	Full frame	9 / 3
	SPARS10	143	Full frame	9 / 3
	SPARS25	353	Full frame	9 / 3
	SPARS50	703	Full frame	9 / 3
	SPARS100	1403	Full frame	9 / 3
	SPARS200	2803	Full frame	9 / 3
IR01S04	STEP25	249	Full frame	6 / 3
	STEP50	449	Full frame	6 / 3
	STEP100	799	Full frame	6 / 3
	STEP200	1399	Full frame	6 / 3
	STEP400	2799	Full frame	6 / 3
IR01S05	MIF600	600	Full frame	3 / 3
	MIF900	900	Full frame	3 / 3
	MIF1200	1200	Full frame	3 / 3
	MIF1500	1500	Full frame	3 / 3
IR05S01	RAPID	0.9, 1.7, 4.2, 12.8	64, 128, 256, 512	2 / 4
	SPARS10	100, 101, 103, 112	64, 128, 256, 512	2 / 4

Table 1: Details of the data analyzed as part of our readnoise analysis.

Analysis

The analysis of these data follows exactly that of the IR channel readnoise data from TV2 testing (Hilbert, 2008). The discussion of effective noise comes directly from that document.

Prior to analyses, all data ramps were run through several steps of the WFC3 IDL data reduction pipeline (Hilbert, 2004). We used the vertical inboard reference pixels to subtract the bias signal from each ramp. The standard practice of subtracting the initial read from all subsequent reads in a ramp was not performed. The reason for this is discussed below. Finally, we put each ramp into units of electrons by applying a gain of 2.26 e-/ADU. This value combines the gain value of 2.6 e-/ADU derived from TV3 data, along with an intra-pixel capacitance (IPC) correction factor of 0.87, also derived from TV3 data. No non-linearity corrections were necessary due to the low overall signal levels in the data. Finally a bad pixel mask was applied to all the data. This mask was derived from TV3 data, and includes hot/dead pixels, as well as pixels found to lie more than 3σ from the mean in the initial read of the detector. This resulted in just over 5% of the active science pixels being marked as bad. After the initial data reduction, we used the data listed in Table 1 to calculate and report 2 types of readnoise values for the IR channel.

CDS READNOISE

Correlated double sampling (CDS) noise is the most commonly quoted readnoise measure for multiple readout detectors, and refers to the noise associated with the difference of 2 reads of the array. By taking the difference of two consecutive reads, we remove pixel-to-pixel variations in the zero level, leaving behind only noise effects. This technique works best on ramps with short exposure times between reads. This minimizes the amount of dark current that accumulates on the detector, limiting the amount of shot noise in the reads. Noise associated with the readout of the detector should then be the dominant noise source in these difference images.

We measured the CDS readnoise in frames constructed from the differences of consecutive reads in each ramp. For a 16-read ramp, we created 15 consecutive-difference images. We created a histogram of each quadrant in each difference image. The width of a Gaussian fit to each histogram then provided a measure of the noise in that quadrant/image. On a quadrant-by-quadrant basis for each ramp, the median of the histogram widths for all 15 images was recorded as the CDS readnoise for that ramp. The median of the CDS readnoise values for each sample sequence is listed in Table 2.

Figure 1 shows a typical histogram and fit for one quadrant of a difference image. Figure 2 shows the measured CDS readnoise generated from all 15 difference images of a single ramp, in order to provide information on the uncertainty in the measurement. The scatter in the CDS values is dominated by binning and Gaussian fitting effects on the histograms, and represents the uncertainty of the values reported in Table 2.

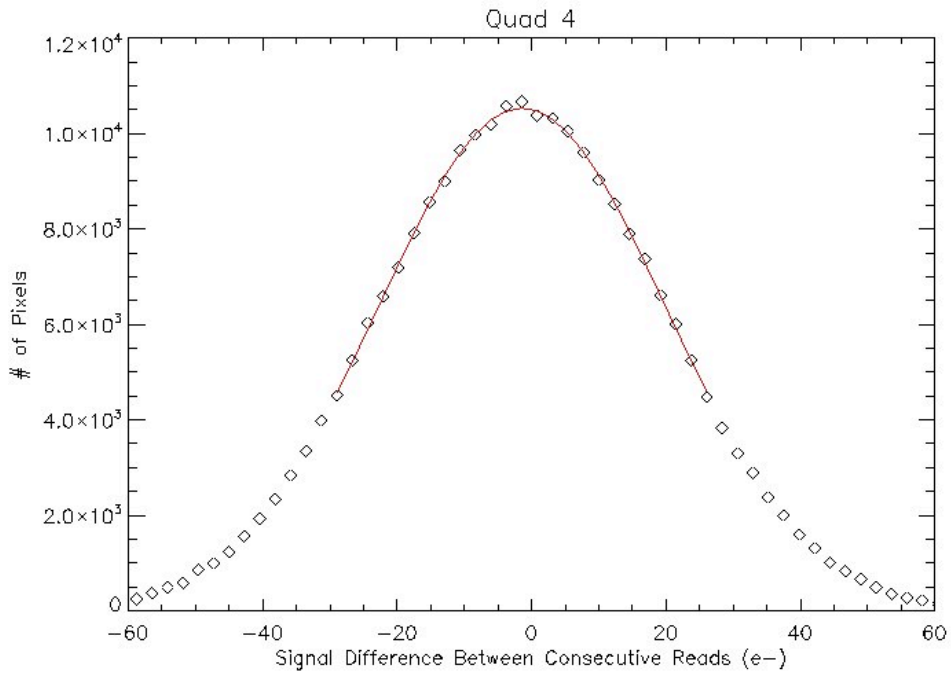


Figure 1: Typical readnoise histogram, from the difference of two consecutive reads in a SPARS200 ramp. The readnoise is the width of the best-fit Gaussian.

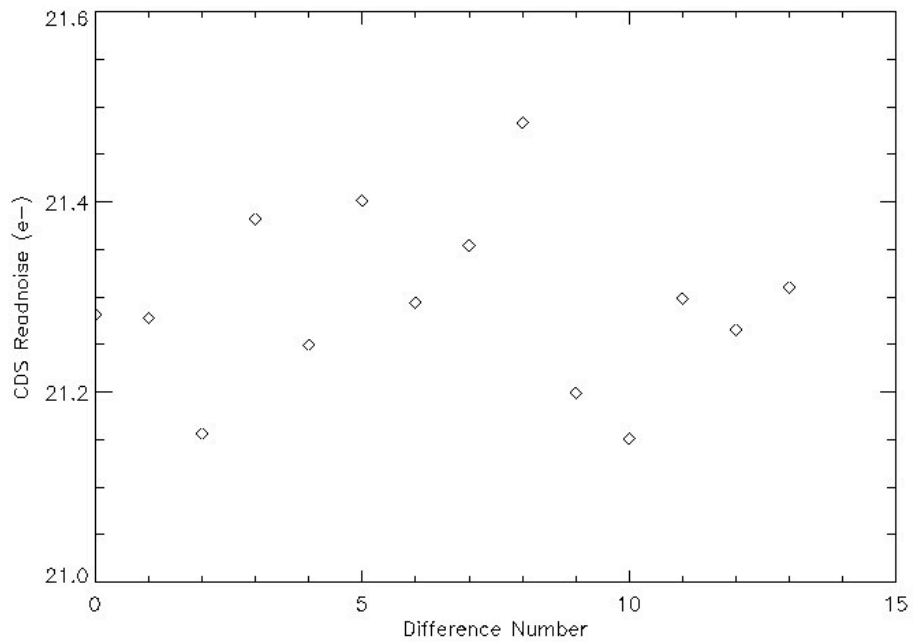


Figure 2: CDS readnoise measured in each difference image associated with a RAPID TV3 ramp in quadrant 1.

The median CDS readnoise value for each sample sequence is given in Table 2. Assuming errors equivalent to the scatter in Figure 2 ($\sim 0.4 e^-$), we see that when using the side 1 electronics of WFC3, quadrant 3 consistently has the lowest readnoise, although the values are similar to those in quadrants 1 and 2 when the uncertainties are considered. Quadrant 4 consistently has significantly higher noise than the other 3 quadrants. Using the side 2 electronics, the noise values in all 4 quadrants are comparable, with quadrant 1 displaying very slightly higher values than the other quadrants.

The increase of the readnoise between sample sequences is greater than expected in some cases. For the longest sample sequence, the SPARS200 ramps, a dark current of $0.02 e^-/\text{sec}/\text{pixel}$ should add $1.3 e^-$ of noise to the $20.3 e^-$ CDS readnoise measured in the RAPID ramps, which is in line with observations. However, the same dark current in the SPARS100 ramps should add only $0.65 e^-$, rather than the $0.9 e^-$ observed increase. The difference between the calculated and observed cases is within the uncertainty of the CDS values.

		CDS Readnoise (e^-)			
SMS	Sample Sequence	Quad 1 MEB1/MEB2	Quad 2 MEB1/MEB2	Quad 3 MEB1/MEB2	Quad 4 MEB1/MEB2
IR01S03	RAPID	20.3 / 20.2	20.4 / 19.8	20.2 / 19.9	21.0 / 20.1
	SPARS10	20.6 / 20.5	20.6 / 20.0	20.4 / 20.1	21.2 / 20.3
	SPARS25	20.8 / 20.7	20.9 / 20.2	20.6 / 20.3	21.4 / 20.5
	SPARS50	21.0 / 20.9	21.0 / 20.5	20.8 / 20.5	21.5 / 20.7
	SPARS100	21.2 / 21.2	21.3 / 20.7	21.0 / 20.7	21.8 / 20.9
	SPARS200	21.6 / 21.5	21.7 / 21.2	21.4 / 21.0	22.1 / 21.2
		Subarray Size (pixels)			
		64x64 MEB1/MEB2	128x128 MEB1/MEB2	256x256 MEB1/MEB2	512x512 MEB1/MEB2
IR05S01	RAPID	16.9 / 16.6	16.9 / 17.0	18.3 / 17.6	20.6 / 20.1
	SPARS10	20.9 / 20.6	20.7 / 20.5	20.8 / 20.4	21.0 / 20.6

Table 2: Median CDS readnoise values, calculated from the median of all CDS values for a given sample sequence/MEB.

EFFECTIVE READNOISE

Line-fitting Data Reduction

A second measure of the readnoise was also made for each ramp. For a ramp taken with the WFC3 IR channel, one of the final data products is a “final image”, in which the individual reads of a data ramp are used to create an image of the signal rate in each pixel. For all of the ramps listed in Table 1, we calculated the effective readnoise in this final image.

We employed a method described by Roberto (priv. communication). During the data reduction process, the “final image” for a ramp is created using line-fitting of the measured signal. The best-fit slope measures the signal rate, and the uncertainty associated with this slope represents the effective noise in the final image. In order to find this uncertainty, we began with the uncertainty associated with the original measured signals in each read, and propagated these errors through the final image creation.

This was done via a two-step fitting process, on a pixel-by-pixel basis. First, we calculated a best-fit line to the signal up the ramp, just as if we were creating a “final image”. The slope from this best fit was recorded as the dark current rate for that pixel. Knowing the dark current rate, along with the exposure time for each read within the ramp, we were able to calculate the signal in each read due to dark current accumulation. The shot noise associated with this dark current signal was then the square root of that signal. The other noise component present in the measured signal was the readnoise. For this, we used the median CDS readnoise values listed in Table 1. These CDS noise values could be translated into single-read readnoise values by dividing by the square root of 2, as CDS noise values are calculated on the difference of 2 reads.

Once we knew the values for the two noise components, we combine them in order to obtain a total noise value for each read. However, the readnoise and dark current noise cannot simply be added in quadrature, due to correlation in the dark current values as you travel up the ramp. This implies that the noise associated with the accumulating dark current increases following Equation 1, which was derived by Roberto (2007), where it is Equation 1.50. Here, DC is the measured dark current rate, t is the exposure time, and N is the number of reads in the ramp (16 in our case).

$$\sigma_{DC} = \sqrt{DC \cdot t \cdot \frac{6(N^2 + 1)}{5(N^2 - 1)}} \quad 1)$$

Combining this equation for the dark current shot noise with the readnoise, we arrive at Equation 2, which describes the total noise, or uncertainty, on the measurement of each

signal up the ramp. Here, σ_{CDS} is the CDS readnoise measured using the difference images.

$$\sigma_s = \sqrt{\left(\frac{\sigma_{\text{CDS}}}{\sqrt{2}}\right)^2 + \left(\text{DC} \cdot t \cdot \frac{6(N^2 + 1)}{5(N^2 - 1)}\right)^2} \quad 2)$$

With the noise values from Equation 2 in hand, we repeated the line fitting up the ramp. This time, the noise values were used as the uncertainties associated with the signal values to be fit. In this case, along with the best-fit slope, we were able to calculate the true error on the best-fit slope. All line-fitting was performed on the measured signal versus time, so we took this error on the fitted slope and multiplied by the exposure time of the final read to produce the effective noise. This entire process was performed on a pixel-by-pixel basis, resulting in a map of the effective noise across the entire detector. Also, as there is no rule stating that the “final image” must be constructed from 16 reads of the detector, we repeated this process, varying the number of reads each time. In other words, we performed the line-fitting first using only the first 4 reads of each ramp, in order to find the effective noise on a 4-read ramp. Next, we used 5 reads, then 6, and so on, in order to monitor how the effective noise decreases with the number of reads. As with the CDS images discussed above, once we had an effective noise map, we produced a histogram, and used a Gaussian fit to find the peak value of the distribution.

Figure 3 shows the behavior of the effective noise for one of the SPARS50 ramps versus the number of reads used to produce the final image. The blue line marks the measured CDS readnoise for the ramp. The red curve displays the effective noise measured in a “final image” created from the number of individual reads on the x axis. The effect of using multiple reads for noise reduction is powerful. For any sample sequence, the effective noise decreases by 30-50% in using 16 reads versus 3.

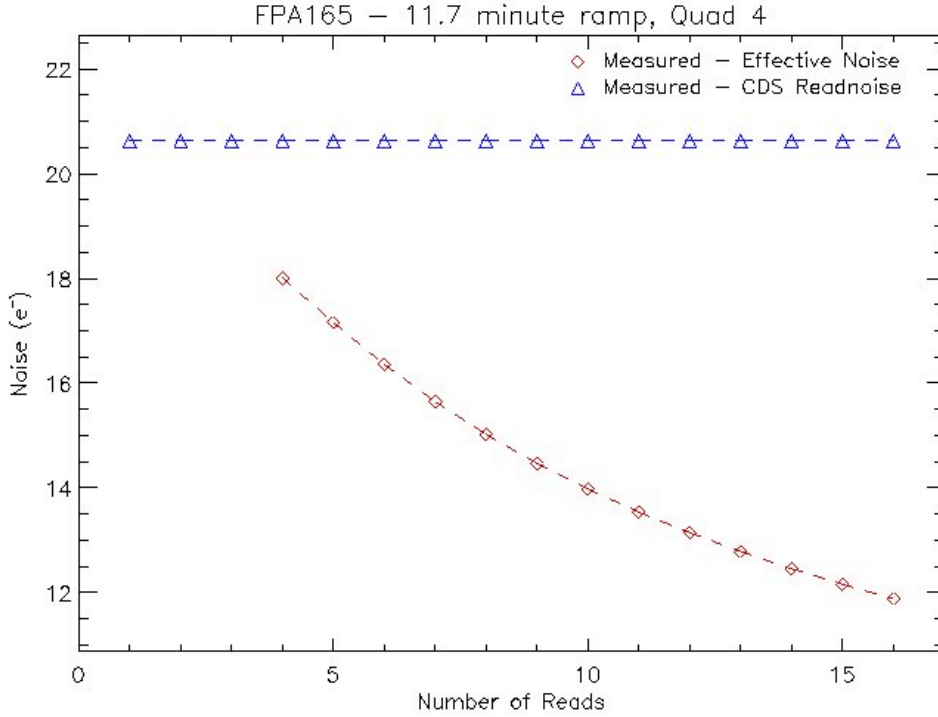


Figure 3: Effective noise for a SPARS50 ramp, versus the number of reads used to create the final image.

Table 3 gives the results of the effective noise measurements in quadrant 4 for each type of sample sequence. The reported noise values represent the median of the effective noise values from all ramps in that group. Results for all quadrants can be found in the Appendix.

From Table 3, we see that the STEP and SPARS sample sequences produce similar effective noise values. At higher read numbers, the noise in the STEP data decreases slightly more than that of the SPARS data. However, the MIF data show an even more dramatic decrease in effective noise between 8 and 16 reads. Using all 16 reads in a ramp, the MIF sample sequences exhibit noise values 2.0 – 4.5 e^- below those in the STEP and SPARS sequences. This is due to the fact that the MIF sequences sample the signal on the detector many times at the beginning and end of a ramp, helping to reduce the uncertainty in the signal at these points. Figure 4 shows the reduction in effective noise for a MIF600 ramp. The measured noise reduction in this plot (red line) is more complex than that in Figure 3 due to the sampling scheme. For 4 through 7 read ramps, the final image was created only from the bias reads in the ramp. The sampling interval was regular at this point, with 2.9 seconds between each read and the next. Reads 8 through 10 were collected in the middle of the ramp, with a long time between the final bias read and first intermediate read. The initial 7 reads were all collected within 17 seconds of the beginning of the ramp. Adding read 8, collected 143 seconds later, to the line-fitting causes the error on the line-fitting to increase. Reads 11 through

16 are the signal reads in the ramp. As with the bias reads, these signal reads were all collected within 17 seconds of one another, and have the highest signal-to-noise of all the reads. Once these were included in the line-fitting, the effective noise began to decrease more quickly than before.

Sample Sequence	Exposure Time for 3/8/16 reads (sec)	Effective Noise 3 Reads (e)	Effective Noise 8 reads (e)	Effective Noise 16 reads (e)
RAPID	6 / 21 / 44	20.3	15.5	11.7
SPARS10	13 / 63 / 143	20.1	15.3	11.7
SPARS25	28 / 153 / 353	19.2	15.1	11.6
SPARS50	53 / 303 / 703	18.9	15.3	12.1
SPARS100	102 / 602 / 1402	19.4	16.0	12.8
SPARS200	202 / 1202 / 2802	19.5	16.5	13.6
STEP25	6 / 74 / 274	20.3	15.3	10.5
STEP50	6 / 99 / 499	20.1	15.8	10.4
STEP100	6 / 99 / 899	20.2	16.0	11.0
STEP200	6 / 99 / 1599	20.4	16.1	11.7
STEP400	6 / 99 / 2799	20.2	16.0	12.6
MIF600	6 / 160 / 600	21.0	16.9	8.6
MIF900	6 / 235 / 900	21.0	16.8	8.7
MIF1200	6 / 310 / 1200	21.0	16.8	8.8
MIF1500	6 / 385 / 1500	20.9	16.8	8.9
Fowler Data Reduction				
		2 Fowler Pairs	4 Fowler Pairs	6 Fowler Pairs
MIF600	588 / 594 / 600	17.2	14.3	13.1
MIF900	888 / 894 / 900	17.8	15.1	14.0
MIF1200	1188 / 1194 / 1200	18.7	15.9	15.0
MIF1600	1488 / 1494 / 1500	18.9	16.7	15.9

Table 3: Effective noise values for various sample sequences, in quadrant 4 of IR4, using MEB1. Results for the other quadrants can be found in the appendix. The Fowler data reduction results are discussed in a subsequent section.

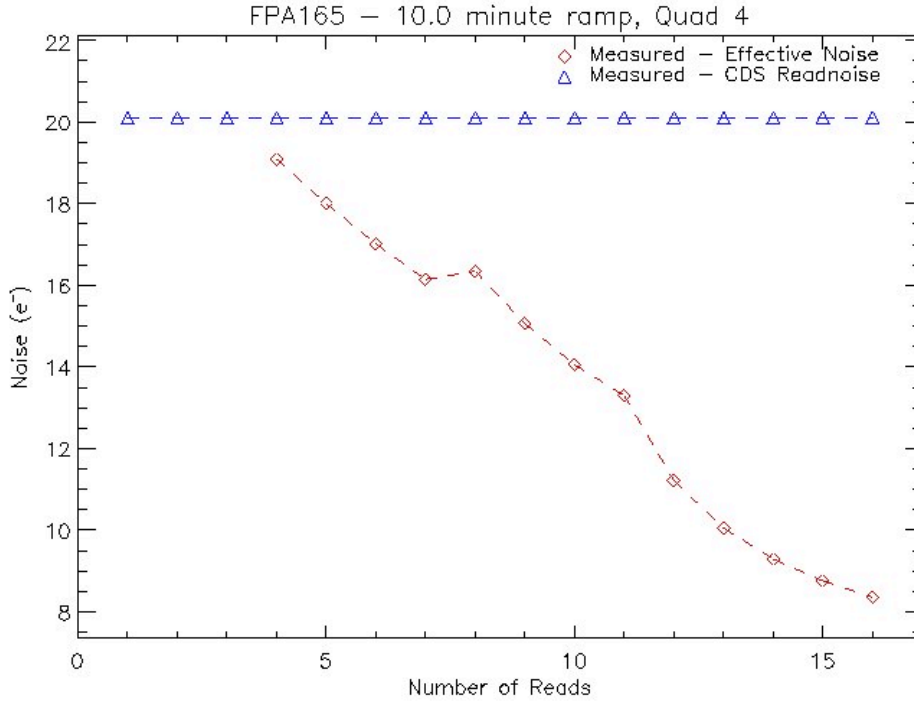


Figure 4: Same as Figure 3, but for a MIF600 ramp. Note the three distinct regions of the red line, which denote the three distinct sample timing regimes within the ramp.

Fowler Data Reduction

At the bottom of Table 3, we present another measure of effective noise. In this case, we use the MIF data, and produce a final image using the Fowler data reduction technique (Fowler & Gatley, 1991). Traditional Fowler sampling measures the signal on the detector many times at the beginning of the ramp, creating a set of “bias reads”, and then an equal number of times at the end of the ramp, creating a set of “signal reads”. Each bias read is then subtracted from the corresponding signal read (ie the first bias read is subtracted from the first signal read), to create a “Fowler pair image”. A final image is then created by taking the pixel-by-pixel medians of the Fowler pair images. For more detail on Fowler sampling and data reduction, see Garnett & Forrest (1993). Data collected using our MIF sample sequences is more like a hybrid Fowler/multiaccum data collection strategy. In addition to a set of bias reads and signal reads, each MIF ramp contains 3 reads taken in the middle of the ramp (Petro, 2006), in order to aid in the removal of cosmic ray effects. The reason for this difference is to aid in the removal of cosmic ray effects. However, this also means that there were three reads in each MIF ramp that could not be used to create Fowler pair images. For the purposes of this readnoise study, we chose to ignore these three reads. For this reason, we were only able to create 6 Fowler pair images from each ramp.

Once we had created final images using the Fowler technique, we calculated effective noise values by fitting Gaussians to histograms of the final images, and

collecting the Gaussian widths. These are the values reported in Table 3. These values show that the Fowler data reduction technique produces effective noise values that are comparable to or slightly higher than those from the line-fitting technique described previously. In Figure 5, we show how the effective noise averages down with number of Fowler pairs for a MIF600 ramp. For 6 pairs, the ramp in Figure 5 produced a final image with $13 - 13.75 e^-$, depending on quadrant. This is comparable to the noise associated with a 12-read SPARS50 ramp, as seen in Figure 3. For the longer MIF sequences, the 6-pair Fowler noise increases by up to $3 e^-$. However, the noise associated with the longer STEP and SPARS sample sequences increases by only $1 e^-$ from that same SPARS50 level. This suggests that regardless of sample sequence, line-fitting is preferable to the Fowler pair reduction technique for reducing WFC3 IR MIF data.

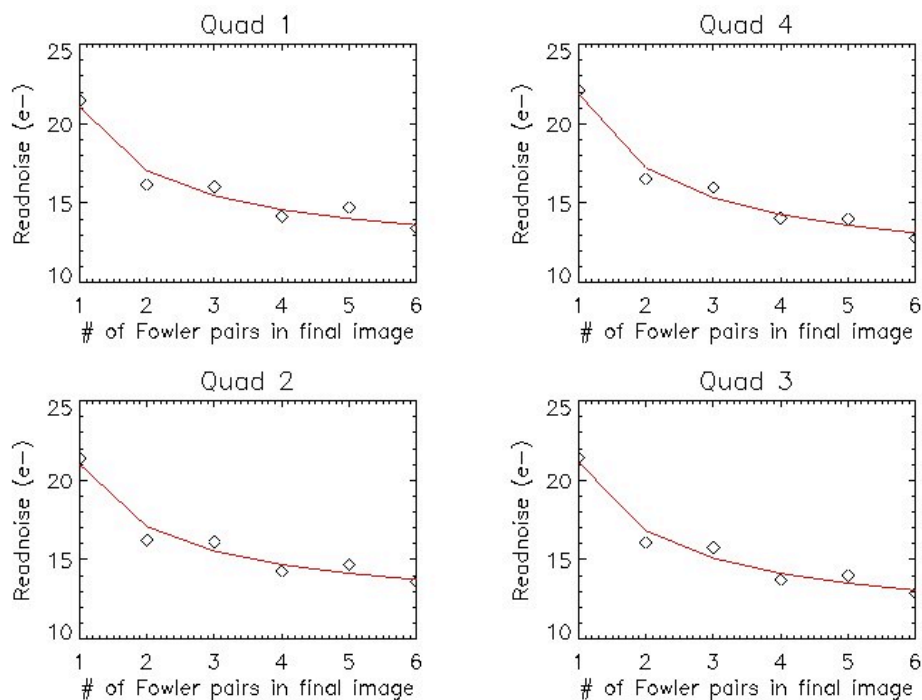


Figure 5: Effective noise in a MIF600 ramp versus the number of Fowler pairs used to create the final image. The black diamonds show the measured noise values, while the red line is from Equation 1.81 in Roberto, 2007, and shows the expected noise values, scaled to our CDS readnoise and flux values.

Conclusions

The readnoise behavior for IR-4 (FPA165) appears fairly complex. CDS readnoise values vary from quadrant to quadrant and (electronics) side to side by roughly 6%. Quadrant 4 has noticeably higher readnoise compared to the other three quadrants when side 1 electronics are used.

Following the standard data reduction practice of creating a final image from the component reads of each ramp, we see that the effective noise for the flight IR detector decreases significantly for large numbers of reads. This implies that for readnoise-

limited observations, maximizing the number of reads in each ramp can be an effective technique for optimizing the signal-to-noise ratio of the data. CDS readnoise values in the IR channel are in the 20 – 21 e^- range. However, using all 16 reads in a ramp to create a final image results in effective noise values between 8.5 and 17 e^- , depending on sample sequence and quadrant.

It appears that the most effective way to minimize the effective readnoise in the final image when in a readnoise-limited regime is to collect data using MIF sample sequences with at least 12 reads, and to reduce this data using the line-fitting technique, rather than Fowler data reduction.

References

Fowler, A. M. and Gatley, I. 1991, SPIE 1541, 127.

Garnett, J. D. & Forrest, W. J. 1993, Proc. SPIE 1946, 395.

Hilbert, B., *WFC3 TV2 Testing: IR Channel Read Noise*. WFC3 ISR 2008-04.
<http://www.stsci.edu/hst/wfc3/documents/ISRs/WFC3-2008-04.pdf> 22 Feb 2008 .

Hilbert, B. *Basic IDL Data Reduction Algorithm for WFC3 IR and UVIS Channel*. WFC3 ISR 2004-10.
<http://www.stsci.edu/hst/wfc3/documents/ISRs/WFC3-2004-10.pdf> 10 June 2004.

Hilbert, B. *WFC3 TV2 Testing: IR Channel Gain Results*.
<http://www.stsci.edu/hst/wfc3/documents/ISRs/WFC3-2007-28.pdf> 5 Dec 2007.

Hilbert, B. and M. Robberto. *WFC3-IR Thermal Vacuum Testing: IR Channel Dark Current*.
<http://www.stsci.edu/hst/wfc3/documents/ISRs/WFC3-2005-25.pdf> 22 Aug 2005.

Petro, L. and T. Wheeler. *New IR Detector Sample Times*.
<http://www.stsci.edu/hst/wfc3/documents/ISRs/WFC3-2006-06.pdf> 2 Oct 2006.

Robberto, M. *Analysis of the sampling schemes for WFC3-IR*.
<http://www.stsci.edu/hst/wfc3/documents/ISRs/WFC3-2007-12.pdf> 30 Apr 2007.

Appendix

Measured effective noise values for each quadrant of the flight detector.

Quadrant 1

Sample Sequence	Exposure Time for 3/8/16 reads (sec)	Effective Noise 3 Reads (°e) MEB1/MEB2	Effective Noise 8 reads (°e) MEB1/MEB2	Effective Noise 16 reads (°e) MEB1/MEB2
RAPID	6 / 21 / 44	19.6 / 19.3	15.0 / 14.8	11.3 / 11.1
SPARS10	13 / 63 / 143	19.6 / 19.1	14.9 / 14.5	11.4 / 11.1
SPARS25	28 / 153 / 353	18.6 / 18.8	14.7 / 14.9	11.2 / 11.4
SPARS50	53 / 303 / 703	18.4 / 18.4	14.9 / 15.0	11.8 / 11.9
SPARS100	102 / 602 / 1402	18.8 / 18.5	15.6 / 15.4	12.6 / 12.6
SPARS200	202 / 1202 / 2802	19.3 / 19.8	16.4 / 16.9	13.6 / 14.1
STEP25	6 / 74 / 274	19.6 / 19.4	14.8 / 14.6	10.2 / 10.1
STEP50	6 / 99 / 499	19.5 / 19.4	15.3 / 15.3	10.0 / 10.0
STEP100	6 / 99 / 899	19.6 / 19.5	15.6 / 15.4	10.8 / 10.8
STEP200	6 / 99 / 1599	19.7 / 19.5	15.6 / 15.5	11.5 / 11.5
STEP400	6 / 99 / 2799	19.5 / 19.5	15.4 / 15.5	12.6 / 12.8
MIF600	6 / 160 / 600	20.3 / 20.3	16.5 / 16.5	8.4 / 8.5
MIF900	6 / 235 / 900	20.4 / 20.3	16.4 / 16.4	8.5 / 8.6
MIF1200	6 / 310 / 1200	20.3 / 20.3	16.4 / 16.4	8.6 / 8.7
MIF1500	6 / 385 / 1500	20.3 / 20.3	16.5 / 16.5	8.8 / 8.8
	Number of Fowler Pairs			
		2 pairs	4 pairs	6 Pairs
MIF600	588 / 594 / 600	17.0 / 17.3	14.5 / 14.9	13.5 / 13.9
MIF900	888 / 894 / 900	17.8 / 18.0	15.6 / 15.8	14.8 / 15.0
MIF1200	1188 / 1194 / 1200	18.5 / 18.7	16.7 / 16.9	16.0 / 16.2
MIF1500	1488 / 1494 / 1500	19.2 / 19.4	17.6 / 17.9	16.9 / 17.3

Table 7: Effective noise values for various sample sequences, in quadrant 1.

Quadrant 2

Sample Sequence	Exposure Time for 3/8/16 reads (sec)	Effective Noise 3 Reads (°e)	Effective Noise 8 reads (°e)	Effective Noise 16 reads (°e)
RAPID	6 / 21 / 44	19.7 / 19.3	15.0 / 14.8	11.3 / 11.1

SPARS10	13 / 63 / 143	19.6 / 19.1	14.9 / 14.5	11.4 / 11.1
SPARS25	28 / 153 / 353	18.6 / 18.8	14.6 / 14.9	11.3 / 11.4
SPARS50	53 / 303 / 703	18.5 / 18.4	14.9 / 15.0	11.8 / 11.9
SPARS100	102 / 602 / 1402	18.9 / 18.5	15.7 / 15.4	12.6 / 12.6
SPARS200	202 / 1202 / 2802	19.3 / 19.8	16.3 / 16.9	13.5 / 14.1
STEP25	6 / 74 / 274	19.7 / 19.0	14.8 / 14.3	10.2 / 9.9
STEP50	6 / 99 / 499	19.6 / 19.0	15.4 / 14.9	10.1 / 9.8
STEP100	6 / 99 / 899	19.6 / 19.0	15.5 / 15.0	10.7 / 10.5
STEP200	6 / 99 / 1599	19.8 / 19.0	15.6 / 15.1	11.4 / 11.2
STEP400	6 / 99 / 2799	19.6 / 18.9	15.5 / 15.0	12.4 / 12.3
MIF600	6 / 160 / 600	20.4 / 19.9	16.5 / 16.1	8.4 / 8.3
MIF900	6 / 235 / 900	20.4 / 19.9	16.4 / 16.0	8.5 / 8.4
MIF1200	6 / 310 / 1200	20.4 / 19.9	16.4 / 16.1	8.6 / 8.5
MIF1500	6 / 385 / 1500	20.4 / 19.9	16.4 / 16.1	8.7 / 8.6
		Number of Fowler Pairs		
		2 pairs	4 pairs	6 Pairs
MIF600	588 / 594 / 600	17.1 / 17.0	14.7 / 14.9	13.7 / 14.0
MIF900	888 / 894 / 900	18.0 / 17.9	16.1 / 16.1	15.3 / 15.5
MIF1200	1188 / 1194 / 1200	19.1 / 18.9	17.5 / 17.5	16.9 / 17.0
MIF1500	1488 / 1494 / 1500	19.9 / 19.9	18.9 / 18.7	18.5 / 18.4

Table 8: Effective noise values for various sample sequences, in quadrant 2.

Quadrant 3

Sample Sequence	Exposure Time for 3/8/16 reads (sec)	Effective Noise 3 Reads (e)	Effective Noise 8 reads (e)	Effective Noise 16 reads (e)
RAPID	6 / 21 / 44	19.5 / 19.3	14.9 / 14.8	11.2 / 11.1
SPARS10	13 / 63 / 143	19.4 / 19.1	14.8 / 14.5	11.3 / 11.1
SPARS25	28 / 153 / 353	18.4 / 18.8	14.5 / 14.9	11.1 / 11.4
SPARS50	53 / 303 / 703	18.2 / 18.4	14.8 / 15.0	11.7 / 11.9
SPARS100	102 / 602 / 1402	18.7 / 18.5	15.4 / 15.4	12.5 / 12.6
SPARS200	202 / 1202 / 2802	19.2 / 19.8	16.4 / 16.9	13.5 / 14.1
STEP25	6 / 74 / 274	19.5 / 19.2	14.6 / 14.4	10.1 / 10.0
STEP50	6 / 99 / 499	19.5 / 19.1	15.2 / 14.9	10.0 / 9.8

STEP100	6 / 99 / 899	19.5 / 19.1	15.4 / 15.2	10.6 / 10.6
STEP200	6 / 99 / 1599	19.5 / 19.0	15.4 / 15.1	11.3 / 11.3
STEP400	6 / 99 / 2799	19.4 / 19.0	15.3 / 15.0	12.3 / 12.4
MIF600	6 / 160 / 600	20.2 / 19.9	16.3 / 16.2	8.3 / 8.3
MIF900	6 / 235 / 900	20.2 / 19.9	16.2 / 16.2	8.4 / 8.4
MIF1200	6 / 310 / 1200	20.2 / 20.0	16.2 / 16.2	8.5 / 8.6
MIF1500	6 / 385 / 1500	20.2 / 19.9	16.3 / 16.3	8.6 / 8.7
	Number of Fowler Pairs			
		2 pairs	4 pairs	6 Pairs
MIF600	588 / 594 / 600	16.8 / 16.9	15.1 / 14.5	13.1 / 13.5
MIF900	888 / 894 / 900	17.4 / 17.7	15.0 / 15.6	14.1 / 14.9
MIF1200	1188 / 1194 / 1200	17.9 / 18.3	15.9 / 16.5	15.1 / 15.8
MIF1500	1488 / 1494 / 1500	18.5 / 19.0	16.7 / 17.6	16.0 / 17.1

Table 9: Effective noise values for various sample sequences, in quadrant 3..

Quadrant 4

Sample Sequence	Exposure Time for 3/8/16 reads (sec)	Effective Noise 3 Reads (e)	Effective Noise 8 reads (e)	Effective Noise 16 reads (e)
RAPID	6 / 21 / 44	20.3 / 19.2	15.5 / 14.7	11.7 / 11.1
SPARS10	13 / 63 / 143	20.1 / 19.0	15.3 / 14.5	11.7 / 11.1
SPARS25	28 / 153 / 353	19.2 / 18.6	15.1 / 14.6	11.6 / 11.3
SPARS50	53 / 303 / 703	18.9 / 18.4	15.3 / 15.0	12.1 / 11.9
SPARS100	102 / 602 / 1402	19.4 / 18.4	16.0 / 15.3	12.8 / 12.4
SPARS200	202 / 1202 / 2802	19.5 / 19.4	16.5 / 16.5	13.6 / 13.8
STEP25	6 / 74 / 274	20.3 / 19.3	15.3 / 14.5	10.5 / 10.0
STEP50	6 / 99 / 499	20.1 / 19.2	15.8 / 15.2	10.4 / 9.9
STEP100	6 / 99 / 899	20.2 / 19.3	16.0 / 15.3	11.0 / 10.6
STEP200	6 / 99 / 1599	20.4 / 19.3	16.1 / 15.2	11.7 / 11.3
STEP400	6 / 99 / 2799	20.2 / 19.3	16.0 / 15.3	12.6 / 12.4
MIF600	6 / 160 / 600	21.0 / 20.3	16.9 / 16.5	8.6 / 8.5
MIF900	6 / 235 / 900	21.0 / 20.1	16.8 / 16.3	8.7 / 8.4

MIF1200	6 / 310 / 1200	21.0 / 20.2	16.8 / 16.3	8.8 / 8.6
MIF1500	6 / 385 / 1500	20.9 / 20.2	16.8 / 16.3	8.9 / 8.7
	Number of Fowler Pairs			
		2 pairs	4 pairs	6 Pairs
MIF600	588 / 594 / 600	17.2 / 17.0	14.3 / 14.3	13.1 / 13.2
MIF900	888 / 894 / 900	17.8 / 17.5	15.1 / 15.2	14.0 / 14.4
MIF1200	1188 / 1194 / 1200	18.7 / 18.3	15.9 / 16.2	15.0 / 15.5
MIF1500	1488 / 1494 / 1500	18.9 / 18.7	16.7 / 17.0	15.9 / 16.4

Table 10: Effective noise values for various sample sequences, in quadrant 4 of FPA165.